

## Article

# Electrodeposition of Zn and Cu Nanoparticles into TiO<sub>2</sub> Nanotubes on Ti6Al4V: Antimicrobial Effect against *S. Epidermidis* and Cytotoxicity Assessment

Bruno Ribeiro <sup>1,2,3,\*</sup> , Ruben Offoiach <sup>2</sup>, Claudia Monteiro <sup>4,5</sup>, Miguel R. G. Morais <sup>4,5,6</sup> ,  
M. Cristina L. Martins <sup>4,5,6</sup> , Ana Paula Pêgo <sup>4,5,6</sup> , Elisa Salatin <sup>1</sup>, Lorenzo Fedrizzi <sup>2</sup> and Maria Lekka <sup>7</sup>

<sup>1</sup> LimaCorporate, Via Nazionale 52, 33038 San Danielle del Friuli, Italy

<sup>2</sup> Polytechnic Department of Engineering and Architecture, University of Udine, Via Cotonificio 108, 33100 Udine, Italy

<sup>3</sup> IMDEA Materials Institute, C/Eric Kandell 2, 28906 Madrid, Spain

<sup>4</sup> i3S—Institute for Research and Innovation in Health Sciences, University of Porto, Rua Alfredo Allen 208, 4200-135 Porto, Portugal

<sup>5</sup> INEB, National Biomedical Engineering Institute, University of Porto, Rua Alfredo Allen 208, 4200-135 Porto, Portugal

<sup>6</sup> ICBAS—Institute of Biomedical Sciences Abel Salazar, Universidade do Porto, 4050-313 Porto, Portugal

<sup>7</sup> CIDETEC, Basque Research and Technology Alliance (BRTA), Po. Miramón 196, 20014 Donostia-San Sebastián, Spain

\* Correspondence: bruno.gomes@imdea.org; Tel.: +34-91-549-34-22

**Abstract:** Surface modification of the Ti6Al4V alloy (ASTM grade 5), with the fabrication of vertically oriented TiO<sub>2</sub> nanotubes, has been receiving increasing attention both as a way to provide advanced bioactive features and the ability to act as reservoirs for a localized, controlled drug release. In this work, TiO<sub>2</sub> nanotubes were grown on the surface of a Ti6Al4V alloy through electrochemical anodization. An ethylene glycol-based electrolyte containing 0.5 wt.% NH<sub>4</sub>F and 2.5% (v/v) H<sub>2</sub>O was used. Post-anodizing heat treatments at 500 °C in air atmosphere were performed to achieve a crystalline oxide layer with a higher mechanical stability. Following these treatments, Zn or Cu nanoparticles were incorporated into the nanotubular structures through electrodeposition processes. Then, the antimicrobial performance of the obtained surfaces was assessed against *Staphylococcus epidermidis*, a Gram-positive bacterium common in implant-related infections. Lastly, the cytotoxicity of the produced surface was evaluated against MC3T3-E1 mouse pre-osteoblast cells. In general, Cu-doped TiO<sub>2</sub> nanotubes presented an almost total antimicrobial action, while Zn doped samples had a lower, but still significant antibacterial effect. However, a highly cytotoxic effect against MC3T3-E1 cells was observed on all anodized samples due to the release of vanadium from the alloy. In spite of this, the surface modification reported in this work can be a valid solution for existing commercially available orthopedic implants, considering that similar solutions were already studied in *in vivo* assays.

**Keywords:** TiO<sub>2</sub> nanotubes; electrochemical anodization; electrodeposition; zinc; copper; antimicrobial; antibacterial; *S. Epidermidis*



**Citation:** Ribeiro, B.; Offoiach, R.; Monteiro, C.; Morais, M.R.G.; Martins, M.C.L.; Pêgo, A.P.; Salatin, E.; Fedrizzi, L.; Lekka, M. Electrodeposition of Zn and Cu Nanoparticles into TiO<sub>2</sub> Nanotubes on Ti6Al4V: Antimicrobial Effect against *S. Epidermidis* and Cytotoxicity Assessment. *Micro* **2024**, *4*, 97–116. <https://doi.org/10.3390/micro4010007>

Academic Editor: Hiroshi Furuta

Received: 29 December 2023

Revised: 26 January 2024

Accepted: 29 January 2024

Published: 8 February 2024



**Copyright:** © 2024 by the authors. Licensee MDPI, Basel, Switzerland. This article is an open access article distributed under the terms and conditions of the Creative Commons Attribution (CC BY) license (<https://creativecommons.org/licenses/by/4.0/>).

## 1. Introduction

Titanium (Ti) alloys are widely used as biomaterials in orthopedic implants. In particular, Ti  $\alpha + \beta$  alloys, mainly Ti6Al4V, are commonly used in bone implant devices that require high mechanical strength, such as femoral hip stems, fracture fixation plates, and intramedullary nails or screws. This alloy was adopted due to its superior biocompatibility, low toxicity, good mechanical properties (high strength and low Young's modulus), and excellent corrosion resistance [1–3]. Nevertheless, implant-associated infections still represent a high burden for both patients and healthcare providers, with an increased cost

(up to 3–4 fold) associated with prolonged hospital stays and the need for additional treatments [4,5]. The most common type of microorganism in orthopedic implant-associated infections are bacteria. In general, aerobic Gram-positive bacteria represent 45 to 60% of the cases, while Gram-negative represent 9% of the cases, and anaerobic bacteria represent only 4%. Bacteria from the *Staphylococcus* genus are the most frequent, mainly *Staphylococcus aureus* (*S. aureus*) in the US and *S. epidermidis* in Europe [6,7]. The common strategy to prevent postsurgical infection is the administration of antibiotic agents in systemic prophylaxis. However, the efficiency of this treatment is severely hindered by the relatively low drug concentration that reaches the target site and a potential toxicity, since the antibiotic reaches healthy tissues in high quantities before reaching the place of action [6,8,9]. Furthermore, over the last decades, the common use of antibiotics in medical treatments has resulted in the emergence of an increasing number of antibiotic-resistant strains of pathogens. Through a plethora of mechanisms, either preexisting or resulting from a mutation of chromosomal genes or horizontal gene transfer, microorganisms can inhibit the action of antimicrobial agents, either by active efflux, a reduced permeability of the cell membrane, modification of the target structure, or protection of the antibiotic target [10]. Strains of antibiotic-resistant bacteria have been recovered from clinical cases of implant-associated infections [11,12].

The antimicrobial properties of Ti and Ti alloys can be improved by altering their surface characteristics through either passive or active strategies, allowing for a local antimicrobial action. Passive strategies have the purpose of hindering microbial adhesion, either by killing the microorganisms through contact or by repelling microorganisms from the surface [13–15]. These strategies rely on modification of surface characteristics such as roughness, chemistry (alloying chemistry of the near-surface area), surface energy, potential and conductivity, which are known to influence cellular adhesion [16]. One of these strategies includes surface nano-structuring, which can be achieved through electrochemical anodization for the growth of TiO<sub>2</sub> nanotubes (TNTs), possibly followed by a post-anodizing heat treatment to tailor the crystalline structure of the surface oxide layer [16,17]. TiO<sub>2</sub> nanotubes are known to provide the Ti alloy surface with nanoroughness and superhydrophobicity, which may hinder bacterial adhesion [18,19], as well as photocatalytic properties, if activated by light or UV radiation, which leads to the oxidation of organic matter including bacteria [20,21].

Active strategies rely on the loading or incorporation of antimicrobial agents that possess targeted cytotoxic effects against pathogenic microorganisms [13–15,22]. These substances can either be deposited, in permanent fashion through covalent bonds or be incorporated into biodegradable coatings (such as chitosan or hydroxyapatite) or porous structures with the intention of a controlled, local release over time, killing both at the surface and in the vicinity of the implant [14,22,23]. In this sense, nanoporous structures such as TiO<sub>2</sub> nanotubes, due to their unique tubular geometry, can act as reservoirs and local delivery systems of antimicrobial compounds. Several options for antimicrobial agents have been investigated [24–26]. Antibiotics are the most obvious choice, having a known and well-described efficacy and toxicity after years of use in a clinical setting [13,27,28]. However, they face some issues. First, they are usually targeted to a specific set of microorganisms having a limited spectrum of action, thus requiring the incorporation of other different antibiotic compounds for a larger spectrum. For instance, aminoglycosides, which include gentamicin, are effective against Gram-negative bacilli and have some synergistic activity against some Gram-positive bacteria such as *Staphylococcus* and *Enterococcus* [29].  $\beta$ -lactams, such as penicillin or nafcillin, on the other hand, specifically target Gram-positive bacteria [30,31]. Secondly, as mentioned previously, there is the issue of antibiotic-resistant microorganisms, such as the methicillin-resistant *Staphylococcus aureus*, which render these compounds ineffective [10]. In this regard, synthetic substances like chlorhexidine or antimicrobial peptides could be considered as an alternative. However, these still face the issue of a limited spectrum of action and in the case of antimicrobial peptides, the risk of not being stable enough for their application, having only a limited half-life in the human body [13,17,23].

Inorganic compounds based on silver (Ag) [15,32,33], copper (Cu) [34–36], or zinc (Zn) [37] are a potential alternative. This class of antimicrobial agents comprises ceramic and metallic-based materials as well as their ionic forms or salts, and owe their antimicrobial activity to their ionic or nano form, rather than the bulk material. They have been shown to possess significant broad-spectrum antimicrobial activity (targeting both Gram-positive and Gram-negative bacteria, viruses, and even fungus), being also effective even against antibiotic-resistant microorganisms [14,15,23]. Of these, Ag is the most prevalently used in biomedical applications, having been applied in commercial solutions [15].  $\text{Ag}^+$  interferes with bacterial cell membrane permeability and cellular metabolism. Moreover, these cations can also contribute to the formation of reactive oxygen species [23,38]. Nevertheless, silver is not an element naturally present in the human body, not even at trace concentrations, which raises concerns about exposure and potential toxicity. It is known that silver tends to deposit in a wide range of organs and that in either ionic or nanoform can interfere with biomolecules such as proteins and induce changes in gene and protein expression [15]. A concentration between 1.8% to 6.5 wt% has been found to inhibit bacterial proliferation without decreasing osteoblast activity [13,29,33,39]. Alternatively, Zn and Cu have been described to also possess a broad-spectrum antimicrobial action and have also shown effectiveness against antibiotic-resistant microorganisms. Nevertheless, their antimicrobial action is not as strong as silver, with Cu being the closest and Zn the less effective. For this reason, they have been less explored [14,23,40]. On the other hand, both Zn and Cu should possess better biocompatibility. Cu has a role in bone metabolism with its deficiency being linked to skeletal abnormalities and is reported to inhibit osteoclast activity. Zn is an essential trace element, being present in several tissues of the human body, including the bone mineral phase. It is involved in the stimulation of bone formation by osteoblasts and inhibition of bone resorption by osteoclasts [37,38,41–43].

In a previous work [44], the growth process of TNTs on the surface of a Ti6Al4V alloy through electrochemical anodization was thoroughly described. The effect of applied potential difference, anodization time, and alloy phase composition were analyzed with regard to the resulting morphology and geometry of the nanotubes. Aside from its potential as an antimicrobial reservoir, the possibility of using TNTs as a surface modification for Ti alloys to provide an increased surface area and elicit improved biological responses from mammalian cells has also been explored [24,45–47]. The works of Brammer et al., Zhang et al., and Yu et al. report on an overall improvement in cellular adhesion, proliferation, and differentiation in different human cell types, including bone cells and blood platelets, using nanotubes with an anatase or anatase/rutile crystalline structure [24,48,49]. An extensive literature exists on the structure of anodically produced  $\text{TiO}_2$  nanotubes with regard to the crystallization process by heat treatment [50–53]. It is well known that crystalline TNTs, produced by anodization followed by a subsequent heat-treatment, show an improved mechanical stability, bone cell response, and accelerated apatite formation, as compared to smooth Ti surfaces [54–56]. In this work, Zn and Cu were incorporated through electrodeposition into heat-treated TNTs grown on the surface of a Ti6Al4V alloy under previously analyzed conditions and its biocompatibility and potential antimicrobial effects were assessed.

## 2. Materials and Methods

### 2.1. Ti6Al4V Specimen Preparation

Medical grade Ti6Al4V disks with a diameter of 3 cm and thickness of 0.4 cm were used as substrates for all experiments. Firstly, the disks were ground using SiC papers (grades 800 up to 4000) and then were mechanically polished by cloth, using a silica suspension. After polishing, all samples were ultrasonically degreased and progressively cleaned in ethanol, acetone, and DI water for 5 min each.

Anodic oxidation of the as-polished Ti6Al4V (represented as Ti) samples was carried out as described in our previous work [44]. Briefly, a platinum plate was used as the cathode and an ethylene glycol non-aqueous solution containing 0.5 wt.%  $\text{NH}_4\text{F}$  and 2.5%

*v/v* DI H<sub>2</sub>O, kept at room temperature, was used as an electrolyte. The fabrication of the TiO<sub>2</sub> nanotube layers was carried out at 60 V for 1 h in order to obtain TiO<sub>2</sub> nanotubes with a target diameter between 70–100 nm, as described in a previous work [44]. After performing the anodic oxidation process, the anodized samples were cleaned in acetone for 5 min in an ultrasound bath and air dried. Then, the samples were heat treated at 500 °C for 3 h in order to obtain an anatase crystalline oxide. The anodized and heat-treated samples are represented as TNT.

## 2.2. Antimicrobial Decoration/Functionalization

The decoration of TNTs with Zn or Cu nanoparticles (ZnNPs or CuNPs) was achieved through electrochemical deposition processes. For both compounds, a three-electrode system was used with an Ag/AgCl reference electrode, Pt wire as a counter electrode, and the heat-treated TNTs sample as the working electrode. Before functionalization, cyclic voltammetry was performed prior to deposition to identify the deposition potentials for each compound. For the deposition of Zn, a 3.2 mM Zn(NO<sub>3</sub>)<sub>2</sub> electrolyte was used. Deposition was performed for times of 1, 3, 10, 15 min, at either room temperature or 70 °C, and either under ultrasound or without agitation, to optimize the morphology of the obtained functionalized samples. For deposition of Cu, a 3.2 mM CuSO<sub>4</sub> aqueous solution acidified at pH 2 with H<sub>2</sub>SO<sub>4</sub> was used. Optimization of the morphology of the deposited material was achieved by varying the deposition potential (−0.6 V, −0.8 V and −1 V vs. Ag/AgCl), the deposition time (5, 12, 180, and 360 s), and with or without agitation under ultrasound. The TiO<sub>2</sub> nanotube samples decorated with either Zn or Cu are represented as TNT-Zn or TNT-Cu, respectively.

## 2.3. Surface Analysis

The morphology of the anodized specimens was assessed by field-emission electron microscopy (JEOL model JSM-7610FPlus). The micrographs were captured using secondary electrons collected with an in-lens detector. The chemical composition was determined by energy dispersive X-ray spectroscopy (EDXS, Oxford, UK), taken on the top of the sample surface over a 10 × 10 μm area. As there is no direct method to quantify the deposited amount of Zn or Cu within the tubes due to the complex geometry, the Zn or Cu amount detected by EDXS on the top surface of the specimens was used to compare the different deposition conditions.

## 2.4. Antimicrobial Tests

Prior to the tests, the samples were first cleaned in acetone (10 min under ultrasound, twice), washed 3 times with type 1 water (ultrapure water with resistivity > 18 MW-cm and conductivity < 0.056 S/cm, Milli-Q<sup>®</sup>, Millipore, Burlington, MA, USA), and dried with an argon stream. Then, the samples were sterilized in an ethanol (70%) bath (15 min, twice), and rinsed 3 times with sterile type 1 water and dried in an argon stream in sterile conditions. They were then stored under an argon atmosphere.

### 2.4.1. Bacterial Strain and Medium

The reference strain from the American Type Culture Collection *Staphylococcus epidermidis* (*S. epidermidis*) (ATCC 35984) was maintained in stock at −80 °C. Before the experiments, bacterial cells were grown overnight on tryptic soy agar (TSA) at 37 °C. Afterwards, the bacterial cells were scraped from the agar medium into a liquid medium (Mueller Hinton Broth, Sigma-Aldrich, Burlington, NC, USA) and grown overnight at 37 °C. The resulting suspension was then diluted into a proper density in sterile phosphate buffered saline (PBS—ASTM F2129/1219) before the experiments.

### 2.4.2. In Vitro Antibacterial Assay

The antibacterial activity was evaluated by adding 500 μL of bacterial suspension (2 × 10<sup>5</sup> CFU/mL) in PBS to each sample. After 2 h of incubation at 37 °C under agitation

at 150 rpm, the content of the wells containing bacteria in suspension was collected (supernatant) and serial dilutions of 1:10 (up to  $10^{-3}$ ) were made and plated in TSA plates for the determination of antimicrobial activity. The samples in the well were then washed 3 times with PBS, transferred to 5 mL STARSTEDT tubes containing 500  $\mu$ L of 0.5% Tween 80 in PBS and placed on ice. Then, in sequence, the samples were submitted to ultrasound at 160 W for 15 min, vortexed for 5 min, and submitted again to ultrasound for 15 min, to remove the adherent bacteria from the samples. Between each step, the tubes were placed on ice. The 500  $\mu$ L of 0.5% Tween 80 in PBS was then collected and serially diluted (1:10, up to  $10^{-3}$ ) and plated in TSA plates to quantify the adherent bacteria. All TSA plates were incubated overnight at 37 °C. Finally, the number of viable bacterial colonies were counted to appraise the antimicrobial performance, which was evaluated according to the following equation:

$$R(\%) = B/A \times 100\% \quad (1)$$

where R indicates the relative antibacterial viability, A is the average number of viable bacterial colonies from the control sample (as-polished Ti6Al4V) and B is the average number of viable colonies for a specific functionalized sample.

## 2.5. Mammalian Cell Cytotoxicity Assays

### 2.5.1. Cell Culture

The pre-osteoblast (MCT3T3-E1, ATCC CRL-5293) cell line, established from C57BL/6 mouse calvaria, was cultured in minimum essential medium with  $\alpha$ -modification ( $\alpha$ -MEM, Gibco, New York, NY, USA), with 10% (*v/v*) heat-inactivated (30 min at 56 °C) fetal bovine serum (FBS, Lonza, Basel, Switzerland), and 1% (*v/v*) penicillin/streptomycin (PS 100 $\times$ , Gibco). A cell stock culture was established in a T25 cell culture flask (ThermoFisher Scientific, Waltham, MA, USA) in an incubator at 37 °C, 5% CO<sub>2</sub>, and 95% humid atmosphere. The medium was replaced every 48 h and the cells were trypsinized (0.25% trypsin-EDTA, Gibco, NY, USA) twice a week at pre-confluence.

### 2.5.2. Tests on Extracts

The cytocompatibility was assessed through an indirect test in accordance with the ISO 10993-5 standard [57]. To obtain extracts of each sample, Ti, TNT, TNT-Zn, and TNT-Cu discs were defatted and sterilized as described in Section 2.4 and then incubated in 1.5 mL of  $\alpha$ -MEM supplemented with 1% (*v/v*) PS in an orbital shaker at 37 °C for 24 h at 180 rpm. The extracts were subsequently supplemented with 10% (*v/v*) FBS and serially diluted to 50%, 25%, and 5% (*v/v*) in complete culture medium. Cells were seeded on 24-well tissue culture polystyrene plates (Sarstedt) at a density of  $2 \times 10^4$  viable cells/well (Trypan blue assay) and treated with the extracts and respective serial dilutions, for 24 h. A sample of  $\alpha$ -MEM subjected to the same incubation conditions as those used to obtain the extracts was used as a negative control, while a 1% (*v/v*) Triton X-100 (Sigma-Aldrich, Burlington, NC, USA) solution prepared in fresh culture medium was used as a positive control.

### 2.5.3. Resazurin Assay

The cytotoxicity was assessed by measuring cell metabolic activity through a resazurin assay. Briefly, 10% (*v/v*) of resazurin solution (0.1 mg/mL, in PBS) was added to each well, followed by a 3 h incubation at 37 °C, in a 5% CO<sub>2</sub> and 95% humid atmosphere. Subsequently, 100  $\mu$ L of the medium was transferred into a black-walled 96-well plate (Greiner, Kremsmünster, Austria) and the fluorescence was measured at excitation and emission wavelengths of 530 and 590 nm, respectively (Synergy Mx microplate reader—Biotek Instruments, Winooski, VT, USA).

### 2.5.4. Fluorescence Labeling and Microscopy

After the pre-designated incubation period, the cells were washed with PBS and fixed with 4% (*v/v*) paraformaldehyde (Sigma) in PBS for 15 min. After fixation, the cells were permeabilized with 0.2% Triton X-100 (Sigma) in PBS for 10 min under stirring (50 rpm) in

an orbital shaker. The cell cytoskeleton was stained by treating the cells with Alexa Fluor 488 phalloidin (Invitrogen, Carlsbad, CA, USA) 5 U/mL for 30 min in the dark. The cell nuclei were counterstained with Hoechst 33342 (Invitrogen) for 10 min in the dark. The samples were imaged using an inverted epifluorescence microscope (Leica DMI 6000 FFW, Leica, Wetzlar, Germany) with a 10×/0.25 objective.

### 2.6. Ion Release

The TNT-Zn and TNT-Cu samples were immersed in 5 mL PBS solution, at room temperature. At distinct time points, 1 mL of PBS was removed from each sample for testing and another 1 mL of fresh PBS was added. Samples were taken after 1 h, 2 h, 4 h, 6 h, and 1, 2, 3, 4, 7, 11, 14, 17, and 21 days of immersion. The Zn or Cu ions released per 1 mL of PBS at each timepoint were quantified by inductively-coupled plasma-atomic emission spectroscopy (ICP-AES). For each sample type, 3 individual replicates were performed. In addition, the TNT, TNT-Zn, and TNT-Cu samples were immersed in 5 mL of PBS and stored at room temperature. After 7 days of immersion, a multimetal analysis was performed to determine the release profile of metallic ions in solution.

### 2.7. Statistical Analysis

All in vitro and ion release assays were performed in triplicate and the values are expressed as the mean  $\pm$  standard deviation. Each experiment was replicated three times with data from a typical experiment shown. Statistical differences were calculated by means of a one-way ANOVA combined with the Student-Newman-Keuls post-hoc test. In all statistical evaluations,  $p < 0.05$  was considered highly significant.

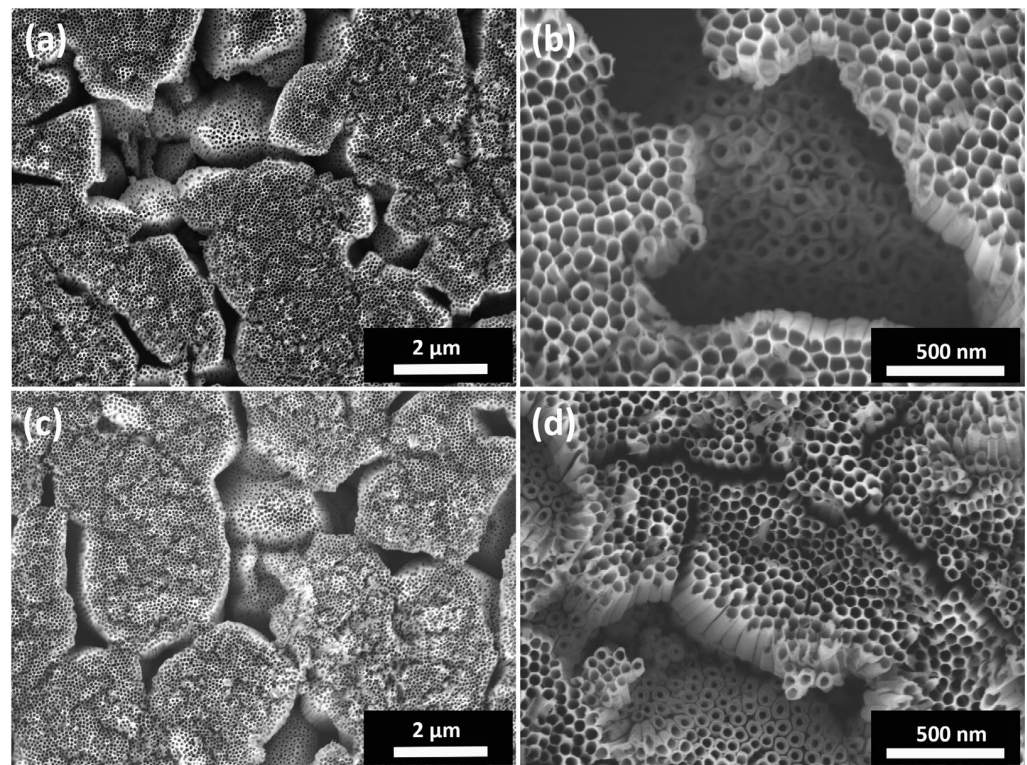
## 3. Results

### 3.1. TiO<sub>2</sub> Nanotube Morphology and Structure

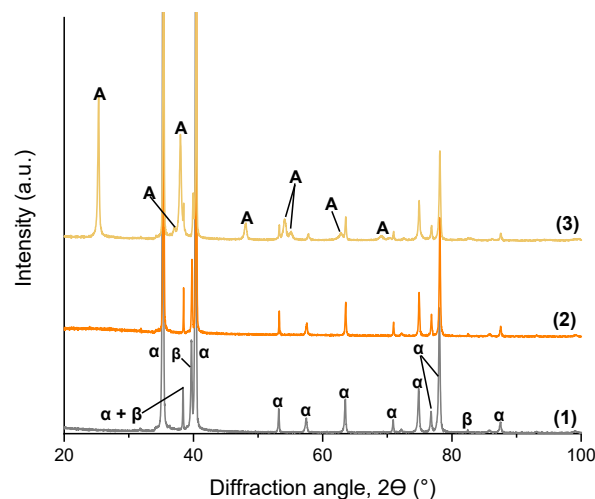
In Figure 1, FESEM micrographs depicting a top view of the obtained TNTs after the anodization and post-anodizing heat treatment processes are shown. As described in our previous work [44], the dual-phase  $\alpha + \beta$  microstructure of the Ti6Al4V substrate led to the formation of a non-uniform anodic oxide layer. Over the Al-rich  $\alpha$ -phase, open and well-defined TNTs were obtained with a honeycomb-like structure and thin tube walls. The diameter of the obtained nanotubes was approximately 105 nm. On the other hand, over the V-rich  $\beta$ -phase, open-top individual nanotubes were also obtained, but they were shorter, presented thicker walls, and had a smaller internal diameter (approximately 65 nm). The specific size of the nanofeatures of the produced nanotubes can impact cell behavior, especially the inner diameter of the nanotubes [45,58]. This diameter-dependent response was confirmed for different cell types, independently of chemistry (verified for TiO<sub>2</sub> and ZrO<sub>2</sub> nanotubes) and crystallization states [58]. However, the triggered response varies depending on the cell. For mesenchymal stem cells, diameters between 15 and 30 nm are optimal for increased cellular adhesion and proliferation as well as for ALP activity and bone matrix deposition. Higher nanotube diameters of around 100 nm induce programmed cell death. For osteoblasts, on the other hand, larger diameters of 70 to 100 nm have been shown to accelerate cellular adhesion, proliferation, ALP activity, and mineralization [45,58]. After heat-treatment, the samples present slightly thicker tube-walls but the overall morphology is not compromised.

Figure 2 presents X-ray diffractograms of as-polished, anodized, and heat-treated at 500 °C for 3 h, Ti6Al4V samples. TiO<sub>2</sub> can either be amorphous or possess a crystalline structure of anatase or rutile. The TiO<sub>2</sub> nanotubes produced through electrochemical anodization are usually amorphous. Only after the post-production annealing treatment do they transition into an anatase or rutile crystalline structure [59–62]. Accordingly, in Figure 2, the as-anodized sample presents the same peaks as the as-polished sample, corresponding to the  $\alpha$ - or  $\beta$ -phase of the alloy, while the heat-treated sample resulted in a crystalline TiO<sub>2</sub>. TiO<sub>2</sub> nanotubes with a crystalline structure, more specifically an

anatase or an anatase/rutile crystalline structure, can improve hydroxyapatite growth and consequently, cell response [54,55,63].



**Figure 1.** FESEM micrographs depicting a top-view of nanotubes as-produced (a,b) and after heat-treatment at 500 °C, for 3 h (c,d).



**Figure 2.** X-ray diffractograms of the Ti6Al4V alloy as-received (1), as-anodized (2), and thermally treated post-anodization at 500 °C for 3 h (3).  $\alpha$  and  $\beta$  refers to the  $\alpha$ - or  $\beta$ -phase of the alloy substrate, respectively, while A refers to the anatase of the crystalline  $\text{TiO}_2$ .

Figure 3 presents the chemical composition of oxides obtained by EDXS for the samples after each surface treatment. As reported in the literature, the as-produced anodic oxide contains small amounts of fluorides, which are only removed via heat-treatment [48,50]. Moreover, the surface treatments led to a change of the O/Ti ratio (wt.%) due to the much thicker surface oxide present after anodization and post-anodizing heat treatment.

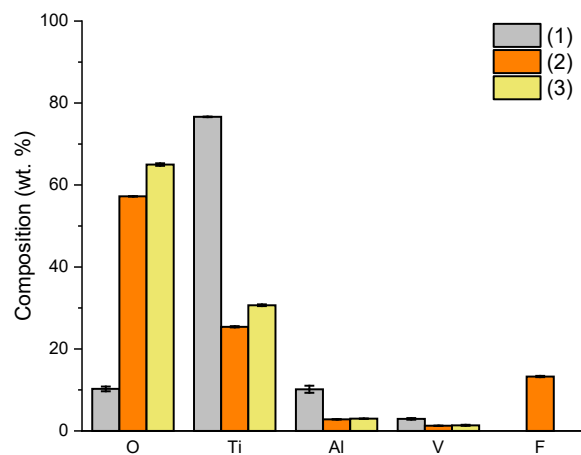


**Figure 3.** Results of the EDXS composition analysis taken on the top of Ti6Al4V alloys surface over a  $10 \times 10 \mu\text{m}$  area in samples as-received (1), as-anodized (2), and thermally treated post-anodization at  $500^\circ\text{C}$  for 3 h (3). The values shown are the mean values of 15 independent measurements.

### 3.2. Electrodeposition of ZnNPs

Figure 4 depicts the cyclic voltammogram, chemical composition, and morphology of the samples obtained after electrodeposition of ZnNPs into  $\text{TiO}_2$  nanotubes on the surface of Ti6Al4V alloys. Figure 4A shows the cyclic voltammogram (CV) obtained in a 3.2 mM  $\text{Zn}(\text{NO}_3)_2$  electrolyte in a three-electrode system using heat-treated TNTs as the working electrode, Pt as the counter, and Ag/AgCl as the reference electrode. The potential was scanned from  $-2$  to  $1.5$  V vs. Ag/AgCl at a scan rate of  $0.1$  V/s. From the CV curve, in accordance with the IUPAC convention [64], a reduction peak of about  $-1$  V vs. Ag/AgCl was identified as the reduction peak of  $\text{Zn}^+$  to Zn. Based on this, the potential of  $-1.6$  V vs. Ag/AgCl was chosen for deposition of Zn (Figure 4A, grey arrow). The deposition potential is in accordance with previous works [65,66].

For process optimization, various experimental parameters were tested, including deposition time (1, 3, 5, 10, 15, and 30 min), agitation conditions (no agitation or ultrasound), and different temperatures (room temperature or a high temperature of  $70^\circ\text{C}$ ). For deposition times less than 10 min, no deposited zinc was detected. On the other hand, for deposition times of 10, 15, or 30 min, the amount of deposited zinc was very similar, approximately  $4.73 \pm 0.15$  wt.%,  $4.83 \pm 0.2$  wt.% and  $3.9 \pm 0.05$  wt.%, respectively, as measured by EDXS on the top surface of the specimens (Figure 4B(1–3)). FESEM micrographs depicting the morphology of the ZnNPs showed that after 10 min of deposition time, they were not uniformly distributed (Figure 4C(a)) with the nanoparticles concentrated in clusters accumulated on the tube tops (Figure 4C(b)). The increase in deposition time to 15 min led to a more uniform distribution over the surface (Figure 4C(c)) with individualized ZnNPs of similar diameter grown on the tube tops (Figure 4C(d)). A further increase of deposition time to 30 min resulted in Zn-deposited particles with a similar morphology (Figure 4C(e,f)). Ultrasound agitation led to the accumulation of what seems to be ZnO/ZnOH over the tube tops, with no individual particle morphology, and resulting in the loss of tubular morphology (Figure 4C(g,h)) and in the deposition of a much higher amount of Zn, about  $35.09 \pm 0.2$  wt.% (Figure 4B(4)). A high temperature of  $70^\circ\text{C}$  should prevent the formation of  $\text{Zn}(\text{OH})_4^{2-}$  and promote the deposition of single well-defined ZnO crystals on top of the tubes [67]. However, it led to a non-uniform distribution of Zn, with no individual particle morphology, in specific zones of the samples as is evidenced by the low magnification micrographs (Figure 4C(i)). A closer look at those zones (Figure 4C(j)) shows that Zn-oxides accumulated on top of the tubes and the nanotubular morphology of the surface was lost. In addition, the amount of deposited Zn was about 3.04 wt.% (Figure 4B(5)), less than the deposition performed at room temperature. Thus, based on these results, the deposition of Zn on  $\text{TiO}_2$  nanotubes was performed at room temperature for 15 min without mixing.

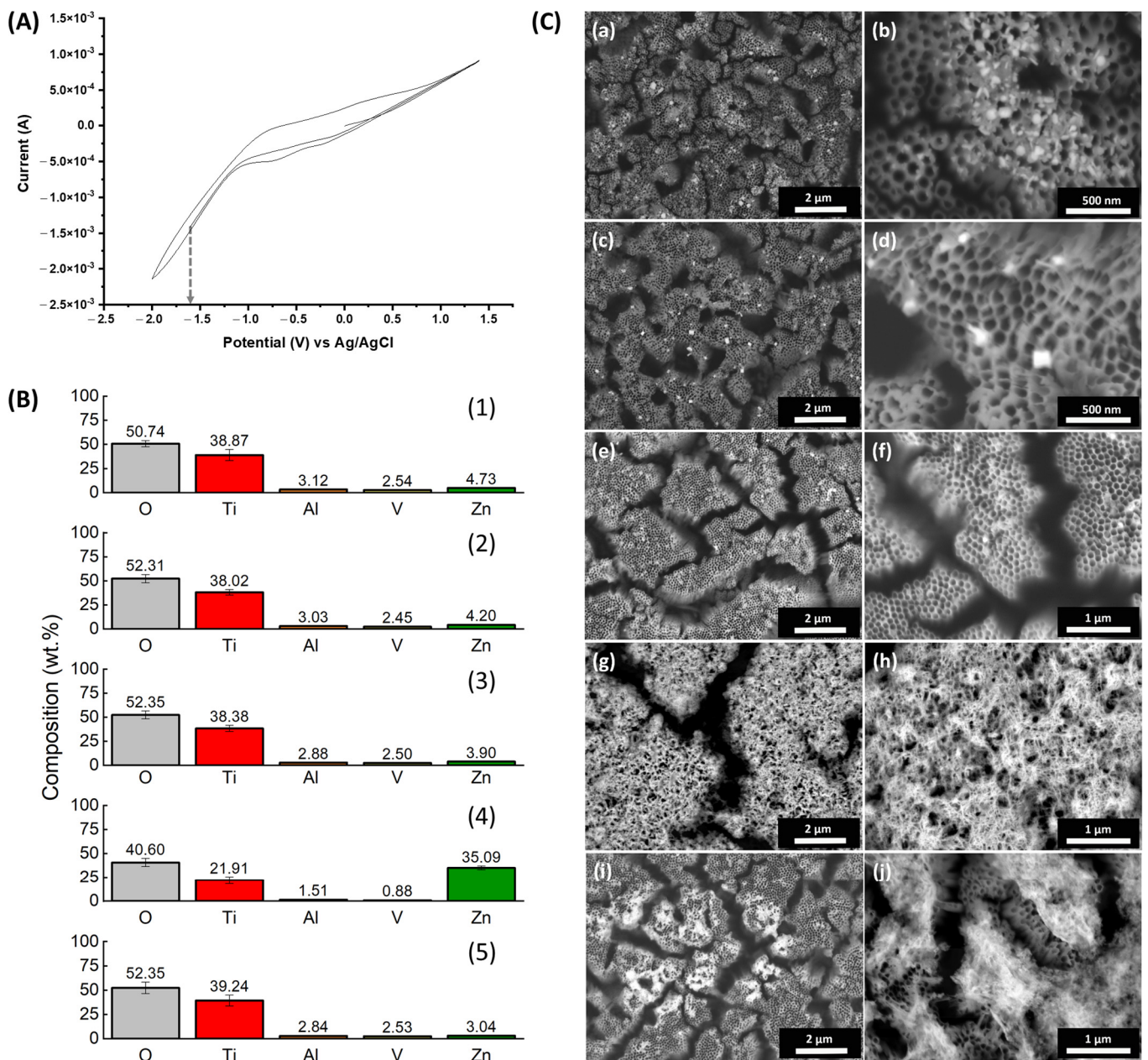


**Figure 4.** Electrodeposition of ZnNPs on anodized Ti6Al4V samples: (A) The cyclic voltammogram obtained in a 3.2 mM  $Zn(NO_3)_2$  on anodized Ti6Al4V samples; the grey arrow indicates the selected potential for the reduction of Zn on the surface of the TNTs sample of  $-1.6$  V vs. Ag/AgCl; (B) The results of EDXS composition analysis taken on the top of the functionalized TNTs surface over a  $10 \times 10 \mu m$  area; the values listed are the mean values of 15 independent measurements. (C) FESEM micrographs depicting a top-view of the nanotubular layer after electrodeposition of ZnNPs. For (B,C): (1),(a,b) deposition for 10 min, at room temperature with no mixing; (2),(c,d) deposition for 15 min, at room temperature with no mixing; (3),(e,f) for 30 min, at room temperature with no mixing; (4),(g,h) deposition for 15 min under ultrasound at room temperature; (5),(i,j) for 15 min, with no mixing at  $70^\circ C$ .

### 3.3. Electrodeposition of CuNPs

Figure 5 depicts the cyclic voltammogram, chemical composition, and morphology of the samples obtained through electrodeposition of CuNPs into the  $TiO_2$  nanotubes produced on the surface of the Ti6Al4V alloy. In Figure 5A, a representative CV curve for the electrodeposition of Cu on heat-treated TNTs at a scan rate of 0.1 V/s and a potential

ranging from  $-2.0$  V to  $0.5$  V in a  $3.2$  mM  $\text{CuSO}_4$  aqueous solution is shown. The electrolyte was a  $\text{CuSO}_4$  solution acidified at pH 2 with  $\text{H}_2\text{SO}_4$  and the deposition was carried out in a three-electrode system using heat-treated TNTs as the working electrode, Pt as the counter, and Ag/AgCl as the reference electrode. Two reduction peaks can be distinguished, a first one at about  $-0.36$  V vs. Ag/AgCl and a second one at about  $-0.8$  V vs. Ag/AgCl. Considering this, for optimization, the deposition of Cu was attempted at different applied potentials ( $-0.6$ ,  $-0.8$  and  $-1$ ), times (90, 180 s), and with or without ultrasound stirring.

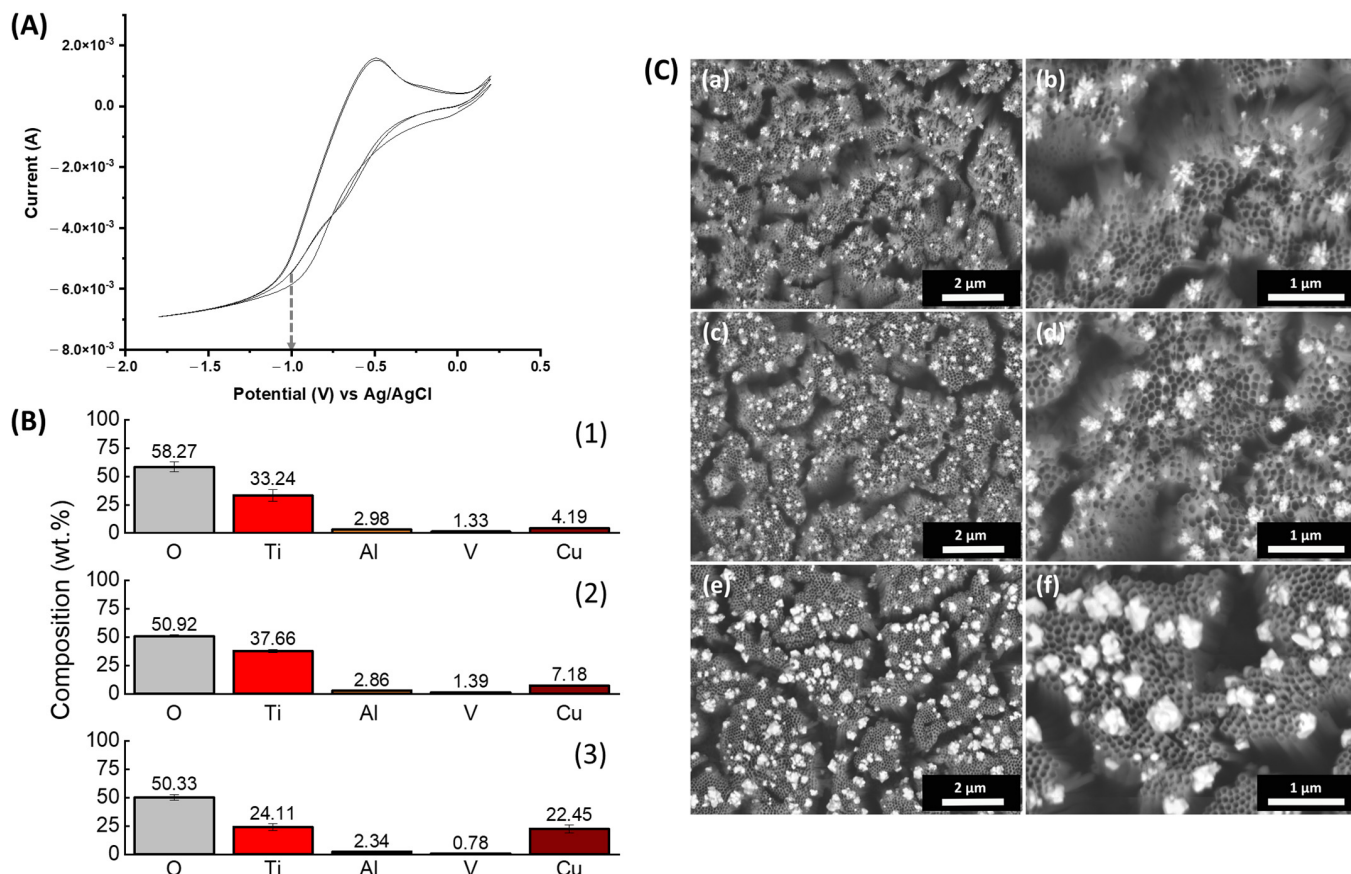


**Figure 5.** Electrodeposition of CuNPs on anodized Ti6Al4V samples: (A) The cyclic voltammogram obtained in a  $\text{CuSO}_4$  solution acidified at pH 2 with  $\text{H}_2\text{SO}_4$  on anodized Ti6Al4V samples; the grey arrow indicates the final selected potential for the reduction of Cu on the surface of the TNTs samples of  $-1$  V vs. Ag/AgCl; (B) The results of EDXS composition analysis taken on the top of the functionalized TNTs surface over a  $10 \times 10 \mu\text{m}$  area. The values listed are the mean values of 15 independent measurements. (C) FESEM micrographs depicting a top-view of nanotubes after electrodeposition of Cu at  $-1$  V vs. Ag/AgCl. For (B,C): (1),(a,b) deposition for 90 s at room temperature with no mixing; (2),(c,d) deposition for 180 s at room temperature with no mixing; (3),(e,f) deposition for 180 s at room temperature under ultrasound.

The morphology of the electrodeposited Cu particles is represented in the micrographs shown in Figure 5C. The amount of deposited Cu is reported in the graphs of Figure 5B, for each condition. No Cu deposition was observed for the deposition performed at  $-0.6$  V vs. Ag/AgCl for 90 s (not shown). For the deposition performed at  $-0.8$  V vs. Ag/AgCl, the amount of Cu deposited was about  $4.06 \pm 0.31$  wt.%, but no nanoparticles were visible on the sample (not shown). For the deposition performed at  $-1$  V vs. Ag/AgCl (Figure 5A, grey arrow), nanoparticles of Cu with a diameter of approximately 250 nm were formed on the top of the tubes. Additionally, the amount of deposited Cu was  $4.06 \pm 0.31$  wt.% (Figure 5B(1),C(a,b)). For this voltage, a longer deposition time of 180 s and agitation with ultrasound were employed. Both the increase in time and in ultrasound led to

an increase in the amount of deposited Cu ( $7 \pm 0.7$  wt.% and  $22.8 \pm 5.5$  wt.%, respectively (Figure 5B(2,3),5C(c,d,e,f)). Morphologically, the increase in deposition time led to a higher amount of CuNPs on the top of the tubes (Figure 5C(b,d,f)). But the nanoparticles had a similar diameter. The application of ultrasounds led to the formation of both bigger nanoparticles and a much higher amount of deposited Cu. Considering these results, a deposition conducted at  $-1$  V vs. Ag/AgCl for 180 s with no mixing, was chosen for functionalization so that an amount comparable to that of Zn could be deposited on the samples.

### 3.4. Antibacterial Activity of Zn- and Cu-Decorated TNTs

The antibacterial activity of Zn- and Cu-decorated TNTs (TNT-Zn and TNT-Cu) was determined through the quantification of viable *S. epidermidis* bacterial cells both in suspension and adhered to the surface of the samples after a 2 h incubation. The results are reported in Figure 6. For the bare Ti6Al4V samples (Ti), the total count in live bacteria cells in suspension was about  $2.2 \times 10^5$  CFU/mL, which is in line with the initial inoculum of  $2 \times 10^5$  CFU/mL. The number of live, adhered *S. epidermidis* was about  $7.82 \times 10^3$  CFU/mL. These results are in accordance with previous works [68] that state the capacity of these particular bacteria species to abundantly adhere to the surface of bare Ti samples. The viability of bacterial cells in the as-polished Ti sample was considered as the base for the calculation of the percentage of viable cells for all of the other samples. The bacterial viability was 92% and 95% for the non-functionalized TNT sample, in suspension or adhered, respectively. These results indicate that in spite of the dual-morphology of the anodic oxide and the presence of microscale cavities on the surface of the anodized sample (Figure 1), the bacterial cell viability is not influenced, either positively or negatively, by the anodization process. Thus, the presence of crystalline anodic TiO<sub>2</sub> nanotubes scale did not seem to exert any antimicrobial effect against *S. epidermidis*, a bacteria known for its adhesion and colonization of surfaces. Several works attest to the antibacterial effect of the nanorough Ti surfaces [18,19] and demonstrate that nanostructures such as TiO<sub>2</sub> nanotubes have contact antibacterial activity [69–71], while other works contest this idea [72]. It is possible that the method used to evaluate the live adhered bacteria in this work is not sufficient to correctly assess bacterial adhesion and viability on the surface of Ti alloys. Further investigation into complete biofilm development may be required to completely elucidate on this issue.

On the other hand, both TNT-Zn and TNT-Cu samples showed a bactericidal effect. The number of viable cells in suspension in PBS after 2 h of incubation with TNT-Zn was significantly reduced to  $1.5 \times 10^5$  CFU/mL or 54.5% of those of the bare Ti. Similarly, the number of viable bacteria adhered to the surface of the sample was about  $4.0 \times 10^3$  CFU/mL, a significant reduction to 63.6% of the viability of those adhered to the Ti6Al4V sample. The susceptibility of *S. epidermidis* to TNT-Zn (in the range of 5.2 wt.%) is in line with the report of Roguska et al., who observed that samples with a “medium” amount of deposited ZnO particles (between 3.8 to 5.2 wt.% of zinc content) obtained after a 3-min electrodeposition process, showed a higher antibacterial activity than samples with 16.4–22.1 wt.% of zinc content, a “high” amount, obtained after a 5-min electrodeposition process. In addition, they observed that the “medium” samples exhibited the highest Zn<sup>2+</sup> release in distilled water. The authors attributed this to the formation of higher and thicker Zn agglomerates on the “high” zinc content samples, which completely covered the top of the TiO<sub>2</sub> nanotubes and had a reduced specific surface area resulting in a lower ion release.

An even greater effect was obtained for the TNTs-Cu samples, which led to 100% loss of bacterial viability, in both planktonic and adhered bacteria. The higher antimicrobial effect of Cu when compared to Zn is reported in the literature and was expected [38,40,73–75].

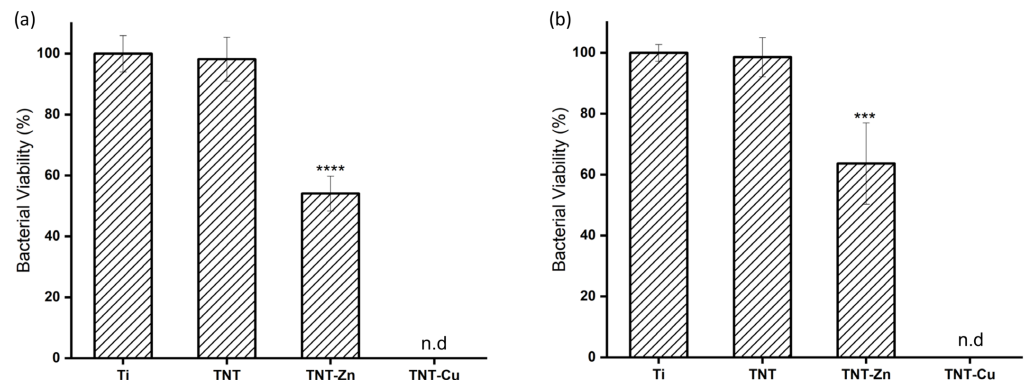


**Figure 6.** The antibacterial efficiency of TNT functionalized with Zn (TNT-Zn) or Cu (TNT-Cu) compared with the as-polished Ti6Al4V alloy (Ti) and anodized and heat-treated Ti6Al4V (TNT), against *S. epidermidis* after 2 h of incubation. (a) Planktonic bacterial viability (b) adherent bacterial viability. “n.d”—no viable bacteria were detected, i.e., 100% loss of bacteria viability. The data is expressed as a percentage of the means  $\pm$  standard deviations ( $n = 5$ ). A One-way ANOVA test was utilized to determine the level of significance against Ti samples: \*\*\*  $p < 0.001$ ; \*\*\*\*  $p < 0.0001$ .

### 3.5. Cytocompatibility Evaluation and Ion Release

To access the cytocompatibility of the functionalized samples, an indirect test was performed in accordance with the ISO 10993-5 standard [57]. Briefly, the prepared samples were incubated in cell culture medium for 24 h at 37 °C and 5% CO<sub>2</sub>. Then the extracts were diluted in fresh cell culture medium to a final concentration of 50% (*v/v*), 25% (*v/v*), and 5% (*v/v*) and the viability of MC3T3-E1 cells was assessed for each of these conditions. The results are shown in Figure 7. As evidenced by fluorescence microscopy images (Figure 7a–t) and the resazurin viability assay (Figure 7u), all anodized and heat-treated samples presented a marked cytotoxic effect towards the cells, independently of the presence of Zn or Cu. The more diluted the extracts, the more the viability of the cells increased. Nevertheless, the presence of Zn on the TNT-Zn conditioned media seemed to somewhat reduce the toxicity of the conditioned media, which can be attributed to its osteogenic properties [76,77]. On the other hand, the presence of Cu on the TNT-Cu conditioned media seemed to have an extra toxic effect towards the cells. To further illustrate this effect, the IC<sub>50</sub> of the extracts obtained for the TNT, TNT-Zn, and TNT-Cu samples is shown in Figure 8. The results show that a viability of at least 50% of the cells is obtained at an extract concentration of 24% (*v/v*) for TNT, 21% (*v/v*) for TNT-Cu, and 35% (*v/v*) for TNT-Zn samples, thus further supporting the results shown in Figure 7. Overall, considering that TiO<sub>2</sub> nanotubes on Ti6Al4V alloys have been deemed cytocompatible to a wide variety of human cells in previous studies, these results were quite surprising [78–81].

To further understand these results, a cumulative metal ion release of the produced samples was performed through ICP-AES. The results are depicted in Figure 9, which shows the cumulative ion release over 21 days for the TNT-Zn and TNT-Cu samples. For both compounds, there is a burst release in less than 24 h of immersion. After this initial burst release, the amount of Cu is quite constant, stabilizing around 0.045 µg/mL. The amount of Zn release, however, increases up to 4 days of immersion (96 h) and the cumulative ion release is overall higher than the amount of copper, due to the higher solubility of Zn in aqueous solutions. It peaks at around 0.12 µg/mL after 3 days of immersion, stabilizing at around 0.072 µg/mL for the remainder of time analyzed. The small variations could be due to replenishing the volume for each sample taken. Considering the results on the antimicrobial activity Zn- and Cu-decorated TNTs described in Section 3.4, these results seem to indicate that Cu can be more effective at lower concentrations than Zn.

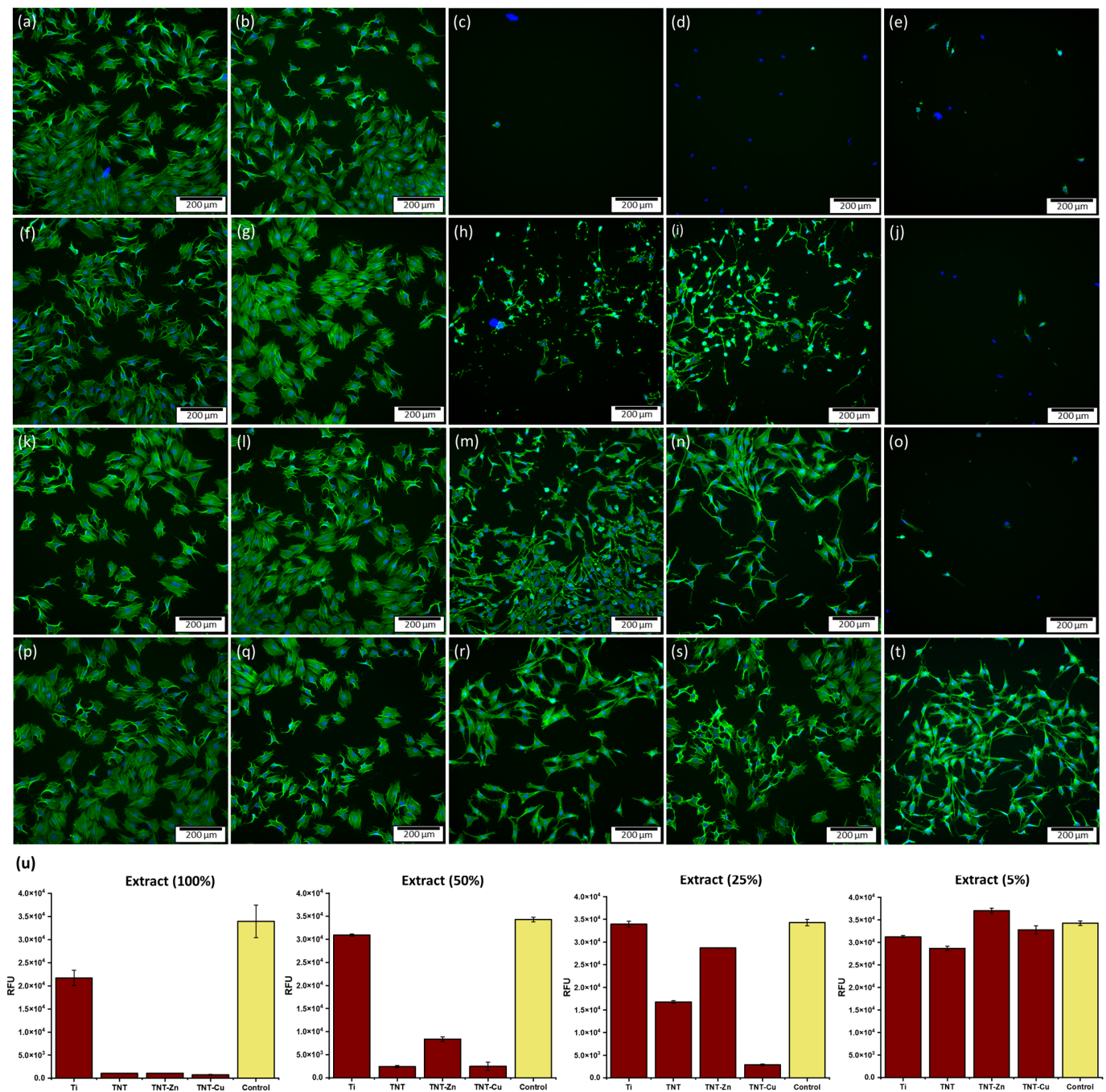


**Figure 7.** Cytotoxicity assessment of Ti, TNT, TNT-Zn, or TNT-Cu samples against MC3T3-E1 pre-osteoblast cells: fluorescence microscopy images detailing cell morphology for (a,f,k,p) control; (b,g,l,q) Ti; (c,h,m,r) TNT; (d,i,n,s) TNT-Zn; and (e,j,o,t) TNT-Cu. Blue—Hoechst and green—f-actin. Overall, anodized samples, independently of the presence of Cu or Zn, presented a marked cytotoxic effect against MC3T3-E1 pre-osteoblast cells. This toxic effect was less evident as the extract was more diluted: (a–e) Extract non-diluted (100%); (f–j) Extract at 50% (v/v); (k–o) Extract at 25% (v/v); (p–t) Extract at 5% (v/v). (u) Results of the resazurin viability tests of the produced samples for each extract dilution.

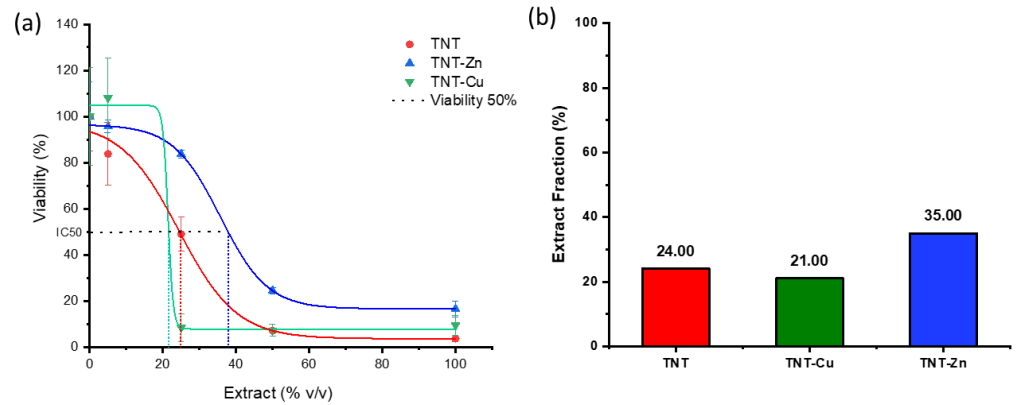


**Figure 8.** The concentration-dependent cytotoxic effect of extracts obtained by incubation of anodized (TNT, red) and functionalized with ZnNPs (TNT-Zn, blue) or CuNPs (TNT-Cu, green) in cell culture medium for 24 h, at 37 °C; (a) dose-response curve (b) extract concentration corresponding to the minimum viability of 50% (IC50) of MC3T3-E1 cells. Viability was measured through the resazurin assay.

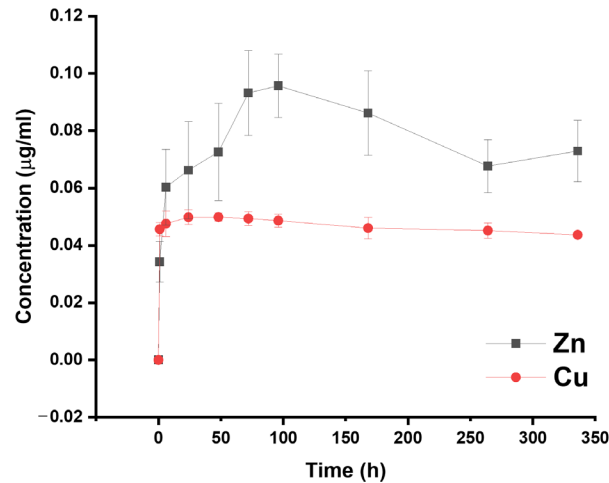


**Figure 9.** The cumulative release of Zn and Cu ions into PBS at room temperature over 21 days of immersion from TNT-Zn and TNT-Cu samples, respectively.

Table 1 shows the results of multimetal analysis obtained by ICP-AES, identifying the concentration of metallic ions in solution after immersing a TNT sample in PBS for 7 days. This test was performed in order to understand the cytotoxic effect observed towards the MC3T3-E1 cells in this study. No amount of Ti or Al (of the alloy) could be detected. However, surprisingly, up to 0.59 µg/mL of vanadium (V) was present in the solution which could explain the observed cytotoxic effect.

**Table 1.** Multimetal analysis of the leachate obtained from TNT samples immersed in PBS for 7 days.

Element	Concentration (µg/mL)
Ti	0
Al	0
V	0.59
Na	4151.00
P	365.3
K	0
Zn	0
Cu	0

Vanadium is a trace element in living organisms, present in very small concentrations in the order of  $10^{-8}$  mol/L. It exerts interesting actions with regard to bone development. While its deficiency in goats has been shown to result in bone deficiency, toxicological studies on its absorption, distribution, and excretion have shown that it tends to accumulate in bone in amounts of up to 10–26  $\mu\text{g/g}$ , replacing phosphate groups in the lattice of hydroxyapatite. Some vanadium derivatives can regulate bone growth, induce morphological alterations, and stimulate glucose consumption. However, it can also have toxic effects. Vanadium compounds have been shown to inhibit the activity of alkaline phosphatase, an enzyme that promotes hard tissue mineralization [82]. In addition, several *in vitro* studies have shown that these compounds can also provoke cell cycle arrest leading to apoptosis [83–85] or in the case of Ti6Al4V alloy, genetic damage [86].

Regarding its effect as an alloying element, Challa et al. reported that MC3T3-E1 cells showed slightly higher cellular attachment, elongation, fibronectin expression, and viability when seeded on the surface of polished specimens of a Ti6Al4Nb alloy compared with the Ti6Al4V alloy. They attributed this behavior to the chemistry of the thin oxide layer of the alloys and the potential leaching of vanadium ions into the media [87]. Barrio et al. reported that Vanadyl (IV) compounds, either free or in complexes with different saccharides such as trehalose, had an inhibitory effect against MC3T3-E1 cells at a concentration of 0.409  $\mu\text{g/mL}$ , independently of the saccharide complex [82,88]. Accordingly, Costa et al. tested the effect of  $\text{V}_2\text{O}_5$  powders at different concentrations on the viability of MC3T3-E1 pre-osteoblast cells. The authors reported that a concentration of 0.022  $\mu\text{g/mL}$  resulted in complete cell death after 48 h and 72 h of incubation time and that at a concentration of 0.221  $\mu\text{g/mL}$ , this effect was observed after 24 h of incubation time [89]. In both of these works, this effect was attributed to the ionic form of vanadium.

Thus, considering these previous studies, the obtained results indicate that V ions are released from the TNT sample in a concentration high enough to cause the death of the MC3T3-E1 cells after 24 h of incubation, an effect that is not observed in the as-polished sample. Vanadium oxide is usually not present in the passive layer of the Ti6Al4V alloy, which mainly consists of  $\text{TiO}_2$  and suboxides ( $\text{TiO}$ ,  $\text{Ti}_2\text{O}_3$ ) as well as  $\text{Al}_2\text{O}_3$  and low levels of metallic hydroxides and oxyhydroxides. This has been observed both on the naturally occurring thin passive film that spontaneously forms on the surface of the alloy [90] as well as on thick flat anodic oxides [91,92]. However, the anodic tubular layer of the samples used in this study presents V-doped  $\text{TiO}_2$  nanotubes, as shown in Figure 1, in accordance with the findings of a previous work [44] later corroborated by others [93]. It is possible that when immersed in cell culture media, V-doped heat-treated anodic oxide preferentially corrodes versus the Al-doped oxide, either due to its stability inherent to the chemical composition or due to a synergistic effect of the recrystallization after heat-treatment, which could have further stabilized the Al-doped oxide. The low stability of V-doped oxide is known [44] and its absence in the titanium oxide electrochemically grown on the surface of the Ti6Al4V alloy when immersed in Hank's solution seems to corroborate this hypothesis [92].

Nevertheless, in the literature, no cytotoxic effect was observed against other commonly used cell types, such as SAOS-2 or MG63 osteoblasts from osteosarcoma, for  $\text{TiO}_2$  nanotubes produced on Ti grade 5 and annealed in similar conditions as reported in this paper [78–81]. This could explain the preferential selection of these cell types for most of the literature reporting on nanotubes grown on this alloy. On the other hand, MC3T3-E1 cells are frequently used for annealed  $\text{TiO}_2$  nanotubes grown on commercially pure Ti alloys with no reports on unexpected cytotoxic effects [49,94,95]. Moreover,  $\text{TiO}_2$  nanotubes produced on the surface of screws and implants of the Ti6Al4V alloy and annealed in similar conditions as described in this work, showed an enhanced bioactivity and osseointegration when implanted *in vivo*, with no cytotoxic effects [96–98]. Human body fluids are rich in organic substances of low molecular weight and polymeric compounds of relatively high molecular weight, such as amino acids, soluble proteins, and traces of cellular debris that may have a role in the concentration of metal ions in the vicinity of the implant. For instance, carbohydrate components of the extracellular matrix and certain proteins possess

anionic functional groups (carboxyl, phosphate, sulphate, glycerate, pyruvate) that bind to metal ions and transport them away from the implant surface, upsetting the equilibrium across the surface double layer that is formed between the electrons on the metal and excess cations in the solution [99,100].

Thus, in spite of these results, the surface modification described in this study could still be considered as a potential solution for the development of antimicrobial coatings on orthopedic implants. Its applicability requires further study, either through *in vivo* assays or *in vitro*, with other bone cell types. Alternatively, this surface modification could be developed and studied in other alloys such as the Ti-6Al-7Nb alloy, which is being considered as an alternative to the Ti6Al4V alloy or other second generation Ti alloys such as the low modulus beta alloys Ti-13Nb-13Zr or Ti-12Mo-6Zr-2Fe [3,87].

#### 4. Conclusions

In this work, the functionalization of anodized Ti6Al4V specimens with well-known antimicrobial agents is thoroughly described. Decoration of annealed TNTs with ZnNPs or CuNPs was achieved through electrochemical deposition processes after optimization of the deposition parameters. In general, under optimized conditions, the obtained samples show nanoparticles of Zn or Cu grown on top of the tubular layers. Parameters such as ultrasound stirring or applied temperature did not allow for a finer distribution alongside nanotube walls.

Antimicrobial assays performed on these samples confirmed the superior antibacterial activity of TNT-Cu samples when compared to TNT-Zn. The use of Cu led to 100% loss of bacteria viability while Zn deposition led to a lower, but still significant antibacterial effect. It becomes clear that Cu is a much more potent antimicrobial agent than Zn.

However, the anodization treatment, followed by annealing at 500 °C for 3 h, led to the formation of surfaces that release toxic amounts of vanadium when in contact with aqueous medium, which led to the death of the MC3T3-E1 mouse pre-osteoblast cells used in this study. To the best of our knowledge, this finding regarding TiO<sub>2</sub> nanotubes produced on the surface of Ti6Al4V alloy has not been reported before. Nevertheless, the existing body of literature has already established that in *in vivo* tests, such surface modification on Ti grade 5 screws and rods results in no major cytotoxic effects and, in addition, presents increased bioactivity and osteointegration. This highlights the need to confirm the cytotoxicity of biomaterials against various cell types for a more complete study. Thus, despite these results, the surface modifications reported in this work can still be a valid solution for existing commercially available orthopedic implants, but further and more complete tests into its cytotoxicity are required.

**Author Contributions:** Conceptualization and methodology: M.L., R.O., A.P.P., C.M. and M.R.G.M.; Data Curation B.R.; Investigation: B.R., R.O., C.M. and M.R.G.M.; Supervision and Project Administration: M.L, E.S., A.P.P., M.C.L.M. and L.F.; Funding Acquisition, M.L.; Writing—original draft, B.R.; Writing-review and editing R.O., E.S., A.P.P., M.R.G.M., C.M. and M.C.L.M. All authors have read and agreed to the published version of the manuscript.

**Funding:** This project has received funding from the European Union’s Horizon 2020 research and innovation programme under the Marie Skłodowska-Curie grant agreement, no. 764977. MRGM acknowledges the support by the Air Force Office of Scientific Research under award number (FA9550-20-1-0417) and FCT—Portuguese Foundation for Science and Technology for his Ph.D. fellowship (2022.13353.BD).

**Institutional Review Board Statement:** Not applicable.

**Informed Consent Statement:** Not applicable.

**Data Availability Statement:** The data that supports the findings of this study are available from the corresponding author (B.R.) upon reasonable request.

**Acknowledgments:** The authors acknowledge the support of the Bioimaging i3S Scientific Platform part of the PPBI—Portuguese Platform of Bioimaging (PPBI-POCI-01-0145-FEDER-022122).

**Conflicts of Interest:** The authors declare no conflict of interest. Bruno Ribeiro and Elisa Salatin are employees of LimaCorporate. The paper reflects the views of the scientists, and not the company.

## References

1. Navarro, M.; Michiardi, A.; Castaño, O.; Planell, J.A. Biomaterials in orthopaedics. *J. R. Soc. Interface* **2008**, *5*, 1137–1158. [[CrossRef](#)]
2. Chen, Q.; Thouas, G.A. Metallic implant biomaterials. *Mater. Sci. Eng. R Rep.* **2015**, *87*, 1–57. [[CrossRef](#)]
3. Geetha, M.; Singh, A.K.; Asokamani, R.; Gogia, A.K. Ti based biomaterials, the ultimate choice for orthopaedic implants—A review. *Prog. Mater. Sci.* **2009**, *54*, 397–425. [[CrossRef](#)]
4. Kapadia, B.H.; Berg, R.A.; Daley, J.A.; Fritz, J.; Bhawe, A.; Mont, M.A. Periprosthetic joint infection. *Lancet* **2016**, *387*, 386–394. [[CrossRef](#)]
5. Pirisi, L.; Pennestrì, F.; Viganò, M.; Banfi, G. Prevalence and burden of orthopaedic implantable-device infections in Italy: A hospital-based national study. *BMC Infect. Dis.* **2020**, *20*, 337. [[CrossRef](#)]
6. Arciola, C.R.; Campoccia, D.; Montanaro, L. Implant infections: Adhesion, biofilm formation and immune evasion. *Nat. Rev. Microbiol.* **2018**, *16*, 397–409. [[CrossRef](#)]
7. Donlan, R.M.; Costerton, J.W. Biofilms: Survival mechanisms of clinically relevant microorganisms. *Clin. Microbiol. Rev.* **2002**, *15*, 167–193. [[CrossRef](#)] [[PubMed](#)]
8. Sui, J. Surface Bio-Functionalization of Anti-Bacterial Titanium. *Coatings* **2022**, *12*, 1125. [[CrossRef](#)]
9. Esteban, J.; Vallet-Regí, M.; Aguilera-Correa, J.J. Antibiotics-and heavy metals-based titanium alloy surface modifications for local prosthetic joint infections. *Antibiotics* **2021**, *10*, 1270. [[CrossRef](#)]
10. Blair, J.M.A.; Webber, M.A.; Baylay, A.J.; Ogbolu, D.O.; Piddock, L.J.V. Molecular mechanisms of antibiotic resistance. *Nat. Rev. Microbiol.* **2015**, *13*, 42–51. [[CrossRef](#)] [[PubMed](#)]
11. Rams, T.E.; Degener, J.E.; Van Winkelhoff, A.J. Antibiotic resistance in human peri-implantitis microbiota. *Clin. Oral Implant. Res.* **2014**, *25*, 82–90. [[CrossRef](#)] [[PubMed](#)]
12. Drago, L.; De Vecchi, E.; Bortolin, M.; Zagra, L.; Romanò, C.L.; Cappelletti, L. Epidemiology and Antibiotic Resistance of Late Prosthetic Knee and Hip Infections. *J. Arthroplast.* **2017**, *32*, 2496–2500. [[CrossRef](#)]
13. Zhao, L.; Chu, P.K.; Zhang, Y.; Wu, Z. Antibacterial coatings on titanium implants. *J. Biomed. Mater. Res.-Part B Appl. Biomater.* **2009**, *91*, 470–480. [[CrossRef](#)]
14. Romanò, C.L.; Scarponi, S.; Gallazzi, E.; Romanò, D.; Drago, L. Antibacterial coating of implants in orthopaedics and trauma: A classification proposal in an evolving panorama. *J. Orthop. Surg. Res.* **2015**, *10*, 157. [[CrossRef](#)] [[PubMed](#)]
15. Milošev, I. Surface Treatments of Titanium with Antibacterial Agents for Implant Applications. In *Biomedical and Pharmaceutical Applications of Electrochemistry*; Springer International Publishing: Cham, Switzerland, 2016; pp. 1–87, ISBN 9783319318479.
16. Moraes, M.N.; da Silveira, W.C.; Teixeira, L.E.M.; Araújo, I.D. Mechanisms of bacterial adhesion to biomaterials. *Rev. Médica Minas Gerais* **2013**, *23*, 99–104. [[CrossRef](#)]
17. Civantos, A.; Martínez-Campos, E.; Ramos, V.; Elvira, C.; Gallardo, A.; Abarrategi, A. Titanium Coatings and Surface Modifications: Toward Clinically Useful Bioactive Implants. *ACS Biomater. Sci. Eng.* **2017**, *3*, 1245–1261. [[CrossRef](#)] [[PubMed](#)]
18. Ellinas, K.; Kefallinou, D.; Stamatakis, K.; Gogolides, E.; Tserepi, A. Is There a Threshold in the Antibacterial Action of Superhydrophobic Surfaces? *ACS Appl. Mater. Interfaces* **2017**, *9*, 39781–39789. [[CrossRef](#)] [[PubMed](#)]
19. Lüdecke, C.; Roth, M.; Yu, W.; Horn, U.; Bossert, J.; Jandt, K.D. Nanorough titanium surfaces reduce adhesion of Escherichia coli and Staphylococcus aureus via nano adhesion points. *Colloids Surf. B Biointerfaces* **2016**, *145*, 617–625. [[CrossRef](#)] [[PubMed](#)]
20. Podporska-Carroll, J.; Panaitescu, E.; Quilty, B.; Wang, L.; Menon, L.; Pillai, S.C. Antimicrobial properties of highly efficient photocatalytic TiO<sub>2</sub> nanotubes. *Appl. Catal. B Environ.* **2015**, *176–177*, 70–75. [[CrossRef](#)]
21. Roy, P.; Kim, D.; Lee, K.; Spiecker, E.; Schmuki, P. TiO<sub>2</sub> nanotubes and their application in dye-sensitized solar cells. *Nanoscale* **2010**, *2*, 45–59. [[CrossRef](#)] [[PubMed](#)]
22. Hetrick, E.M.; Schoenfish, M.H. Reducing implant-related infections: Active release strategies. *Chem. Soc. Rev.* **2006**, *35*, 780–789. [[CrossRef](#)] [[PubMed](#)]
23. Ferraris, S.; Spriano, S. Antibacterial titanium surfaces for medical implants. *Mater. Sci. Eng. C* **2016**, *61*, 965–978. [[CrossRef](#)] [[PubMed](#)]
24. Brammer, K.S.; Frandsen, C.J.; Jin, S. TiO<sub>2</sub> nanotubes for bone regeneration. *Trends Biotechnol.* **2012**, *30*, 315–322. [[CrossRef](#)]
25. Hamlekhan, A.; Sinha-Ray, S.; Takoudis, C.; Mathew, M.T.; Sukotjo, C.; Yarin, A.L.; Shokuhfar, T. Fabrication of drug eluting implants: Study of drug release mechanism from titanium dioxide nanotubes. *J. Phys. D Appl. Phys.* **2015**, *48*, 275401. [[CrossRef](#)]
26. Kazemzadeh-Narbat, M.; Lai, B.F.L.; Ding, C.; Kizhakkedathu, J.N.; Hancock, R.E.W.; Wang, R. Multilayered coating on titanium for controlled release of antimicrobial peptides for the prevention of implant-associated infections. *Biomaterials* **2013**, *34*, 5969–5977. [[CrossRef](#)] [[PubMed](#)]
27. Ghannoum, M.A.; Rice, L.B. Antifungal agents: Mode of action, mechanisms of resistance, and correlation of these mechanisms with bacterial resistance. *Clin. Microbiol. Rev.* **1999**, *12*, 501–517. [[CrossRef](#)]
28. Haleem, A.A.; Rouse, M.S.; Lewallen, D.G.; Hanssen, A.D.; Steckelberg, J.M.; Patel, R. Gentamicin and vancomycin do not impair experimental fracture healing. *Clin. Orthop. Relat. Res.* **2004**, *427*, 22–24. [[CrossRef](#)]
29. Hake, M.E.; Young, H.; Hak, D.J.; Stahel, P.F.; Hammerberg, E.M.; Mauffrey, C. Local antibiotic therapy strategies in orthopaedic trauma: Practical tips and tricks and review of the literature. *Injury* **2015**, *46*, 1447–1456. [[CrossRef](#)]

30. Tarzimoghadam, Z.; Sandlöbes, S.; Pradeep, K.G.; Raabe, D. Microstructure design and mechanical properties in a near- $\alpha$  Ti-4Mo alloy. *Acta Mater.* **2015**, *97*, 291–304. [[CrossRef](#)]
31. Rathbone, C.R.; Cross, J.D.; Brown, K.V.; Murray, C.K.; Wenke, J.C. Effect of various concentrations of antibiotics on osteogenic cell viability and activity. *J. Orthop. Res.* **2011**, *29*, 1070–1074. [[CrossRef](#)]
32. Gallo, J.; Panacek, A.; Pucek, R.; Kriegova, E.; Hradilova, S.; Hobza, M.; Holinka, M. Silver nanocoating technology in the prevention of prosthetic joint infection. *Materials* **2016**, *9*, 337. [[CrossRef](#)] [[PubMed](#)]
33. Lansdown, A.B.G. Silver in Health Care: Antimicrobial Effects and Safety in Use. In *Current Problems in Dermatology*; Karger: Basel, Switzerland, 2006; Volume 33, pp. 17–34.
34. Mehtar, S.; Wiid, I.; Todorov, S.D. The antimicrobial activity of copper and copper alloys against nosocomial pathogens and Mycobacterium tuberculosis isolated from healthcare facilities in the Western Cape: An in-vitro study. *J. Hosp. Infect.* **2008**, *68*, 45–51. [[CrossRef](#)]
35. Ingle, A.P.; Duran, N.; Rai, M. Bioactivity, mechanism of action, and cytotoxicity of copper-based nanoparticles: A review. *Appl. Microbiol. Biotechnol.* **2014**, *98*, 1001–1009. [[CrossRef](#)] [[PubMed](#)]
36. Noyce, J.O.; Michels, H.; Keevil, C.W. Potential use of copper surfaces to reduce survival of epidemic methicillin-resistant Staphylococcus aureus in the healthcare environment. *J. Hosp. Infect.* **2006**, *63*, 289–297. [[CrossRef](#)] [[PubMed](#)]
37. Vijayaraghavan, R. Zinc oxide based Inorganic Antimicrobial agents. *Int. J. Sci. Res.* **2012**, *1*, 35–46.
38. Lemire, J.A.; Harrison, J.J.; Turner, R.J. Antimicrobial activity of metals: Mechanisms, molecular targets and applications. *Nat. Rev. Microbiol.* **2013**, *11*, 371–384. [[CrossRef](#)] [[PubMed](#)]
39. Lansdown, A.B.G. A pharmacological and toxicological profile of silver as an antimicrobial agent in medical devices. *Adv. Pharmacol. Sci.* **2010**, *2010*, 910686. [[CrossRef](#)]
40. Ribeiro, B.; Vázquez-López, A.; Vázquez-Pufleau, M.; Llamasí, M.; Sempere, J.; Yuste, J.; Domenech, M.; Wang, D.-Y.; Vilatela, J.J.; Llorca, J.; et al. Control of microbial agents by functionalization of commercial air filters with metal oxide particles. *Mater. Chem. Phys.* **2024**, *313*, 128684. [[CrossRef](#)]
41. Gao, C.; Li, C.; Wang, C.; Qin, Y.; Wang, Z.; Yang, F.; Liu, H.; Chang, F.; Wang, J. Advances in the induction of osteogenesis by zinc surface modification based on titanium alloy substrates for medical implants. *J. Alloys Compd.* **2017**, *726*, 1072–1084. [[CrossRef](#)]
42. Lowe, N.M.; Fraser, W.D.; Jackson, M.J. Is there a potential therapeutic value of copper and zinc for osteoporosis? *Proc. Nutr. Soc.* **2002**, *61*, 181–185. [[CrossRef](#)]
43. Sadowska, J.M.; Ginebra, M.P. Inflammation and biomaterials: Role of the immune response in bone regeneration by inorganic scaffolds. *J. Mater. Chem. B* **2020**, *8*, 9404–9427. [[CrossRef](#)] [[PubMed](#)]
44. Ribeiro, B.; Offoia, R.; Rahimi, E.; Salatin, E.; Lekka, M.; Fedrizzi, L. On growth and morphology of TiO<sub>2</sub> nanotubes on Ti6Al4V by anodic oxidation in ethylene glycol electrolyte: Influence of microstructure and anodization parameters. *Materials* **2021**, *14*, 2540. [[CrossRef](#)]
45. Tan, A.W.; Pingguan-Murphy, B.; Ahmad, R.; Akbar, S.A. Review of titania nanotubes: Fabrication and cellular response. *Ceram. Int.* **2012**, *38*, 4421–4435. [[CrossRef](#)]
46. Le Guéhennec, L.; Soueidan, A.; Layrolle, P.; Amouriq, Y. Surface treatments of titanium dental implants for rapid osseointegration. *Dent. Mater.* **2007**, *23*, 844–854. [[CrossRef](#)] [[PubMed](#)]
47. Kumar, N.; Chauhan, N.S.; Mittal, A.; Sharma, S. TiO<sub>2</sub> and its composites as promising biomaterials: A review. *BioMetals* **2018**, *31*, 147–159. [[CrossRef](#)] [[PubMed](#)]
48. Zhang, L.; Liao, X.; Fok, A.; Ning, C.; Ng, P.; Wang, Y. Effect of crystalline phase changes in titania (TiO<sub>2</sub>) nanotube coatings on platelet adhesion and activation. *Mater. Sci. Eng. C* **2018**, *82*, 91–101. [[CrossRef](#)] [[PubMed](#)]
49. Yu, W.Q.; Jiang, X.Q.; Zhang, F.Q.; Xu, L. The effect of anatase TiO<sub>2</sub> nanotube layers on MC3T3-E1 preosteoblast adhesion, proliferation, and differentiation. *J. Biomed. Mater. Res. Part A* **2010**, *94*, 1012–1022. [[CrossRef](#)] [[PubMed](#)]
50. Regonini, D.; Jaroenworuluck, A.; Stevens, R.; Bowen, C.R. Effect of heat treatment on the properties and structure of TiO<sub>2</sub> nanotubes: Phase composition and chemical composition. *Surf. Interface Anal.* **2010**, *42*, 139–144. [[CrossRef](#)]
51. Jordanovová, V.; Losertová, M.; Štencek, M.; Lukášová, T.; Martynková, G.S.; Peikertová, P. Microstructure and properties of nanostructured coating on Ti6Al4V. *Materials* **2020**, *13*, 708. [[CrossRef](#)]
52. Rossi, S.; Volgare, L.; Perrin-Pellegrino, C.; Chassigneux, C.; Douset, E.; Eyraud, M. Dual electrochemical treatments to improve properties of Ti6Al4V alloy. *Materials* **2020**, *13*, 2479. [[CrossRef](#)]
53. Regonini, D.; Bowen, C.R.; Jaroenworuluck, A.; Stevens, R. A review of growth mechanism, structure and crystallinity of anodized TiO<sub>2</sub> nanotubes. *Mater. Sci. Eng. R Rep.* **2013**, *74*, 377–406. [[CrossRef](#)]
54. Hilario, F.; Roche, V.; Nogueira, R.P.; Junior, A.M.J. Influence of morphology and crystalline structure of TiO<sub>2</sub> nanotubes on their electrochemical properties and apatite-forming ability. *Electrochim. Acta* **2017**, *245*, 337–349. [[CrossRef](#)]
55. Bai, Y.; Park, I.S.; Park, H.H.; Lee, M.H.; Bae, T.S.; Duncan, W.; Swain, M. The effect of annealing temperatures on surface properties, hydroxyapatite growth and cell behaviors of TiO<sub>2</sub> nanotubes. *Surf. Interface Anal.* **2011**, *43*, 998–1005. [[CrossRef](#)]
56. Das, K.; Bose, S.; Bandyopadhyay, A. TiO<sub>2</sub> nanotubes on Ti: Influence of nanoscale morphology on bone cell-materials interaction. *J. Biomed. Mater. Res. Part A* **2009**, *90*, 225–237. [[CrossRef](#)]
57. ISO 10993-5:2009; Biological Evaluation of Medical Devices—Part 5: Test for In Vitro Cytotoxicity. ISO: Geneva, Switzerland, 2009.
58. Jäger, M.; Jennissen, H.P.; Dittrich, F.; Fischer, A.; Köhling, H.L. Antimicrobial and osseointegration properties of nanostructured titanium orthopaedic implants. *Materials* **2017**, *10*, 1302. [[CrossRef](#)]

59. Regonini, D.; Clemens, F.J. Anodized TiO<sub>2</sub> nanotubes: Effect of anodizing time on film length, morphology and photoelectrochemical properties. *Mater. Lett.* **2015**, *142*, 97–101. [[CrossRef](#)]
60. Kowalski, D.; Kim, D.; Schmuki, P. TiO<sub>2</sub> nanotubes, nanochannels and mesosponge: Self-organized formation and applications. *Nano Today* **2013**, *8*, 235–264. [[CrossRef](#)]
61. Indira, K.; Kamachi Mudali, U.; Rajendran, N. Corrosion behavior of electrochemically assembled nanoporous titania for biomedical applications. *Ceram. Int.* **2013**, *39*, 959–967. [[CrossRef](#)]
62. Bayata, F.; Ürgen, M. Role of aluminum doping on phase transformations in nanoporous titania anodic oxides. *J. Alloys Compd.* **2015**, *646*, 719–726. [[CrossRef](#)]
63. Khrunyk, Y.Y.; Belikov, S.V.; Tsurkan, M.V.; Vyalykh, I.V.; Markaryan, A.Y.; Karabanalov, M.S.; Popov, A.A.; Wysokowski, M. Surface-Dependent Osteoblasts Response to TiO<sub>2</sub> Nanotubes of Different Crystallinity. *Nanomaterials* **2020**, *10*, 320. [[CrossRef](#)] [[PubMed](#)]
64. Elgrishi, N.; Rountree, K.J.; McCarthy, B.D.; Rountree, E.S.; Eisenhart, T.T.; Dempsey, J.L. A Practical Beginner's Guide to Cyclic Voltammetry. *J. Chem. Educ.* **2018**, *95*, 197–206. [[CrossRef](#)]
65. Gallaway, J.W.; Gaikwad, A.M.; Hertzberg, B.; Erdonmez, C.K.; Chen-Wiegart, Y.K.; Sviridov, L.A.; Evans-Lutterodt, K.; Wang, J.; Banerjee, S.; Steingart, D.A. An In Situ Synchrotron Study of Zinc Anode Planarization by a Bismuth Additive. *J. Electrochem. Soc.* **2014**, *161*, A275–A284. [[CrossRef](#)]
66. Shin, S.; Park, C.; Kim, C.; Kim, Y.; Park, S.; Lee, J.H. Cyclic voltammetry studies of copper, tin and zinc electrodeposition in a citrate complex system for CZTS solar cell application. *Curr. Appl. Phys.* **2016**, *16*, 207–210. [[CrossRef](#)]
67. Zoolfakar, A.S.; Rani, R.A.; Morfa, A.J.; Balendhran, S.; O'Mullane, A.P.; Zhuiykov, S.; Kalantar-Zadeh, K. Enhancing the current density of electrodeposited ZnO-Cu<sub>2</sub>O solar cells by engineering their heterointerfaces. *J. Mater. Chem.* **2012**, *22*, 21767–21775. [[CrossRef](#)]
68. Roguska, A.; Belcarz, A.; Pisarek, M.; Ginalska, G.; Lewandowska, M. TiO<sub>2</sub> nanotube composite layers as delivery system for ZnO and Ag nanoparticles—An unexpected overdose effect decreasing their antibacterial efficacy. *Mater. Sci. Eng. C* **2015**, *51*, 158–166. [[CrossRef](#)]
69. Li, Y.; Yang, Y.; Li, R.; Tang, X.; Guo, D.; Qing, Y.; Qin, Y. Enhanced antibacterial properties of orthopedic implants by titanium nanotube surface modification: A review of current techniques. *Int. J. Nanomed.* **2019**, *14*, 7217–7236. [[CrossRef](#)] [[PubMed](#)]
70. Lin, W.T.; Tan, H.L.; Duan, Z.L.; Yue, B.; Ma, R.; He, G.; Tang, T.T. Inhibited bacterial biofilm formation and improved osteogenic activity on gentamicin-loaded titania nanotubes with various diameters. *Int. J. Nanomed.* **2014**, *9*, 1215–1230.
71. Peng, Z.; Ni, J.; Zheng, K.; Shen, Y.; Wang, X.; He, G.; Jin, S.; Tang, T. Dual effects and mechanism of TiO<sub>2</sub> nanotube arrays in reducing bacterial colonization and enhancing C3H10T1/2 cell adhesion. *Int. J. Nanomed.* **2013**, *8*, 3093–3105. [[CrossRef](#)]
72. Yang, Y.; Ao, H.Y.; Yang, S.B.; Wang, Y.G.; Lin, W.T.; Yu, Z.F.; Tang, T.T. In vivo evaluation of the anti-infection potential of gentamicin-loaded nanotubes on titania implants. *Int. J. Nanomed.* **2016**, *11*, 2223–2234. [[CrossRef](#)]
73. Raja, F.N.S.; Worthington, T.; Martin, R.A. The antimicrobial efficacy of copper, cobalt, zinc and silver nanoparticles: Alone and in combination. *Biomed. Mater.* **2023**, *18*, 045003. [[CrossRef](#)]
74. Allizond, V.; Comini, S.; Cuffini, A.M.; Banche, G. Current Knowledge on Biomaterials for Orthopedic Applications Modified to Reduce Bacterial Adhesive Ability. *Antibiotics* **2022**, *11*, 529. [[CrossRef](#)]
75. Akshaya, S.; Rowlo, P.K.; Dukle, A.; Nathanael, A.J. Antibacterial Coatings for Titanium Implants: Recent Trends and Future Perspectives. *Antibiotics* **2022**, *11*, 1719. [[CrossRef](#)]
76. Alves, S.A.; Ribeiro, A.R.; Gemini-Piperni, S.; Silva, R.C.; Saraiva, A.M.; Leite, P.E.; Perez, G.; Oliveira, S.M.; Araujo, J.R.; Archanjo, B.S.; et al. TiO<sub>2</sub> nanotubes enriched with calcium, phosphorous and zinc: Promising bio-selective functional surfaces for osseointegrated titanium implants. *RSC Adv.* **2017**, *7*, 49720–49738. [[CrossRef](#)]
77. Huo, K.; Zhang, X.; Wang, H.; Zhao, L.; Liu, X.; Chu, P.K. Osteogenic activity and antibacterial effects on titanium surfaces modified with Zn-incorporated nanotube arrays. *Biomaterials* **2013**, *34*, 3467–3478. [[CrossRef](#)]
78. Filova, E.; Fojt, J.; Kryslova, M.; Moravec, H.; Joska, L.; Bacakova, L. The diameter of nanotubes formed on Ti-6Al-4V alloy controls the adhesion and differentiation of Saos-2 cells. *Int. J. Nanomed.* **2015**, *10*, 7145–7163. [[CrossRef](#)]
79. Saha, S.; Pramanik, K.; Biswas, A. Antibacterial activity and biocompatibility of curcumin/TiO<sub>2</sub> nanotube array system on Ti6Al4V bone implants. *Mater. Technol.* **2021**, *36*, 221–232. [[CrossRef](#)]
80. Sarraf, M.; Dabbagh, A.; Abdul Razak, B.; Mahmoodian, R.; Nasiri-Tabrizi, B.; Hosseini, H.R.M.; Saber-Samandari, S.; Abu Kasim, N.H.; Abdullah, H.; Sukiman, N.L. Highly-ordered TiO<sub>2</sub> nanotubes decorated with Ag<sub>2</sub>O nanoparticles for improved biofunctionality of Ti6Al4V. *Surf. Coat. Technol.* **2018**, *349*, 1008–1017. [[CrossRef](#)]
81. Swain, S.; Misra, R.D.K.; You, C.K.; Rautray, T.R. TiO<sub>2</sub> nanotubes synthesised on Ti-6Al-4V ELI exhibits enhanced osteogenic activity: A potential next-generation material to be used as medical implants. *Mater. Technol.* **2021**, *36*, 393–399. [[CrossRef](#)]
82. Barrio, D.A.; Etcheverry, S.B. Vanadium and bone development: Putative signaling pathways. *Can. J. Physiol. Pharmacol.* **2006**, *84*, 677–686. [[CrossRef](#)] [[PubMed](#)]
83. Gonçalves, A.P.; Videira, A.; Soares, P.; Máximo, V. Orthovanadate-induced cell death in RET/PTC1-harboring cancer cells involves the activation of caspases and altered signaling through PI3K/Akt/mTOR. *Life Sci.* **2011**, *89*, 371–377. [[CrossRef](#)]
84. Montiel-Dávalos, A.; Gonzalez-Villava, A.; Rodriguez-Lara, V.; Montañón, L.F.; Fortoul, T.I.; López-Marure, R. Vanadium pentoxide induces activation and death of endothelial cells. *J. Appl. Toxicol.* **2012**, *32*, 26–33. [[CrossRef](#)] [[PubMed](#)]

85. Zhao, Y.; Ye, L.; Liu, H.; Xia, Q.; Zhang, Y.; Yang, X.; Wang, K. Vanadium compounds induced mitochondria permeability transition pore (PTP) opening related to oxidative stress. *J. Inorg. Biochem.* **2010**, *104*, 371–378. [[CrossRef](#)]
86. Gomes, C.C.; Moreira, L.M.; JSV Santos, V.; Ramos, A.S.; Lyon, J.P.; Soares, C.P.; Santos, F.V.; Bosco, D.; João Del Rei, S. Assessment of the genetic risks of a metallic alloy used in medical implants. *Genet. Mol. Biol.* **2011**, *34*, 116–121. [[CrossRef](#)]
87. Challa, V.S.A.; Mali, S.; Misra, R.D.K. Reduced toxicity and superior cellular response of preosteoblasts to Ti-6Al-7Nb alloy and comparison with Ti-6Al-4V. *J. Biomed. Mater. Res.-Part A* **2013**, *101 Pt A*, 2083–2089. [[CrossRef](#)]
88. Barrio, D.A.; Cattáneo, E.R.; Apezteguía, M.C.; Etcheverry, S.B. Vanadyl(IV) complexes with saccharides. Bioactivity in osteoblast-like cells in culture. *Can. J. Physiol. Pharmacol.* **2006**, *84*, 765–775. [[CrossRef](#)]
89. Costa, B.C.; Tokuhara, C.K.; Rocha, L.A.; Oliveira, R.C.; Lisboa-Filho, P.N.; Costa Pessoa, J. Vanadium ionic species from degradation of Ti-6Al-4V metallic implants: In vitro cytotoxicity and speciation evaluation. *Mater. Sci. Eng. C* **2019**, *96*, 730–739. [[CrossRef](#)]
90. Hierro-Oliva, M.; Gallardo-Moreno, A.M.; González-Martín, M.L. XPS Analysis of Ti6Al4V Oxidation Under UHV Conditions. *Metall. Mater. Trans. A Phys. Metall. Mater. Sci.* **2014**, *45*, 6285–6290. [[CrossRef](#)]
91. Lewandowska, M.; Pisarek, M.; Rozniatowski, K.; Gradzka-Dahlke, M.; Janik-Czachor, M.; Kurzydłowski, K.J. Nanoscale characterization of anodic oxide films on Ti-6Al-4V alloy. *Thin Solid Films* **2007**, *515*, 6460–6464. [[CrossRef](#)]
92. Chávez-Díaz, M.P.; Luna-Sánchez, R.M.; Vazquez-Arenas, J.; Lartundo-Rojas, L.; Hallen, J.M.; Cabrera-Sierra, R. XPS and EIS studies to account for the passive behavior of the alloy Ti-6Al-4V in Hank's solution. *J. Solid State Electrochem.* **2019**, *23*, 3187–3196. [[CrossRef](#)]
93. Ocampo, R.A.; Bedoya Ochoa, N.; Tamayo, J.A.; Botero, C.; Vargas, C.A.; Gómez, M.; Castaño, J.G.; Zuleta Gil, A.A. Formation of highly ordered TiO<sub>2</sub> nanotubes on Ti6Al4V alloys manufactured by electron beam powder bed fusion (E-PBF). *Int. J. Adv. Manuf. Technol.* **2023**, *128*, 257–266. [[CrossRef](#)]
94. Brammer, K.S.; Oh, S.; Cobb, C.J.; Bjursten, L.M.; van der Heyde, H.; Jin, S. Improved bone-forming functionality on diameter-controlled TiO<sub>2</sub> nanotube surface. *Acta Biomater.* **2009**, *5*, 3215–3223. [[CrossRef](#)] [[PubMed](#)]
95. Yu, W.Q.; Zhang, Y.L.; Jiang, X.Q.; Zhang, F.Q. In vitro behavior of MC3T3-E1 preosteoblast with different annealing temperature titania nanotubes. *Oral Dis.* **2010**, *16*, 624–630. [[CrossRef](#)]
96. Salou, L.; Hoornaert, A.; Louarn, G.; Layrolle, P. Enhanced osseointegration of titanium implants with nanostructured surfaces: An experimental study in rabbits. *Acta Biomater.* **2015**, *11*, 494–502. [[CrossRef](#)]
97. Byeon, S.M.; Kim, H.J.; Lee, M.H.; Bae, T.S. Enhancement of bioactivity and osseointegration in Ti-6Al-4V orthodontic mini-screws coated with calcium phosphate on the TiO<sub>2</sub> nanotube layer. *Korean J. Orthod.* **2022**, *52*, 412–419. [[CrossRef](#)]
98. Byeon, S.M.; Jeon, J.; Jang, Y.S.; Jeon, W.Y.; Lee, M.H.; Jeon, Y.M.; Kim, J.G.; Bae, T.S. Evaluation of osseointegration of Ti-6Al-4V alloy orthodontic mini-screws with ibandronate-loaded TiO<sub>2</sub> nanotube layer. *Dent. Mater. J.* **2023**, *42*, 610–616. [[CrossRef](#)] [[PubMed](#)]
99. Manivasagam, G.; Dhinasekaran, D.; Rajamanickam, A. Biomedical Implants: Corrosion and its Prevention—A Review. *Recent Pat. Corros. Sci.* **2010**, *2*, 40–54. [[CrossRef](#)]
100. Manam, N.S.; Harun, W.S.W.; Shri, D.N.A.; Ghani, S.A.C.; Kurniawan, T.; Ismail, M.H.; Ibrahim, M.H.I. Study of corrosion in biocompatible metals for implants: A review. *J. Alloys Compd.* **2017**, *701*, 698–715. [[CrossRef](#)]

**Disclaimer/Publisher's Note:** The statements, opinions and data contained in all publications are solely those of the individual author(s) and contributor(s) and not of MDPI and/or the editor(s). MDPI and/or the editor(s) disclaim responsibility for any injury to people or property resulting from any ideas, methods, instructions or products referred to in the content.